High-frequency Estimation of Rainfall from Thunderstorms via Satellite Infrared and a Long-Range Lightning Network in Europe.

Themis G. Chronis, Emmanouil N. Anagnostou and Tufa Dinku

Department of Civil and Environmental Engineering

University of Connecticut

Storrs, CT 06269

Submitted to *Quarterly Journal of the Royal Meteorological Society*

Submitted: June 2003

Revised: December 2003

Accepted: January 2004

Corresponding Author: Dr. Emmanouil N. Anagnostou, Civil and Environmental Engineering, U-37, University of Connecticut, Storrs, CT 06269, 860-486-6806 (voice), 860-486-2298 (fax), manos@engr.uconn.edu

Summary

A rain retrieval technique (Omvrios[1]) that combines Geo-stationary satellite Infrared (IR) observations and Cloud-to-Ground (CG) lightning information retrieved from a long-range lightning detection network (Zeus) in Europe is presented in this paper. Cloud systems are defined in the IR temperature array by the 255 K isotherm, in a way similar to the clustering approach devised by Arkin (1979). Bulk parameterizations that relate cloud top IR temperature morphological characteristics and CG lightning information (location and flash rate) are used to discriminate rainy from non-rainy cloud systems, and evaluate the convective and stratiform rain areas and associated area-averaged rain rates of the rainy systems. The technique's parameters were calibrated based on collocated and instantaneous rain fields derived from Special Sensor Microwave/Imager (SSM/I) passive microwave data. Retrieved rain estimates are aggregated to 0.1-degree grid resolution and 6-hours temporal accumulation. The technique is validated during the warm season from May to August 2002, based on independent 6-hourly rain accumulation measurements from a network of 700 rain gauges located across Europe. Statistical analysis shows high correlation with gauge rainfall data (0.88) and low overall systematic difference (~5%). Besides the direct gauge validation, Omvrios has been compared to existing passive microwave-calibrated IR rain retrieval techniques. It is shown that lightning information can lead to significant (25%-40%) reduction in the random error of IR retrievals and to a nearly 0.3 increase in correlation with gauges. In terms of systematic differences (retrieval bias), Omvrios is shown to be consistent as conditional and unconditional biases are nearly equal (within 5%), while for the other IR rain retrievals the variation between conditional and unconditional biases was significant (34% -75%).

Keywords: Retrieval, passive microwave, calibration, validation

[1] Omvrios in Greek language means, "Rain discharge," and represents one of the many names attributed to Zeus, the God of Gods.

1. Introduction

Precipitation is probably the most important hydrological parameter that controls water cycle variability. Quantitative information on precipitation is needed for monitoring the climatic state of water stored in the earth, its variability and climatic trends. Moreover precipitation has an important contribution to the heating budget in the form of latent heating and cooling of the atmosphere, which becomes one of the most important driving forces of the global circulation (Simpson et. al, 1988). In addition to water cycle and climate research, the accurate estimation of precipitation is critical to hydro-meteorological applications, such as the short-term precipitation (Alexander et al. 1999) and flood forecasting (Carpenter et al. 2001), and the improvement of water management systems (Georgakakos et al. 1998).

A critical aspect associated with the preceding studies is the need to resolve precipitation variability over large regions with high temporal (of the order of one to six hours) and spatial (0.1 to 0.5 square degrees) resolution. Precipitation estimates over remote areas are available based on passive microwave observations from a limited number of earth-orbiting satellite sensors such as the Special Sensor Microwave/Imager (SSM/I) instrument on the Defense Meteorological Satellite Program (DMSP) satellites, the Advanced Microwave Scanning Radiometer on Earth Observing System (EOS)-AQUA and ADEOS-II satellites and the Microwave Imager (TMI) onboard Tropical Microwave Measuring Mission (TRMM) satellite. In addition to passive microwave observations, TRMM carries the first space borne Precipitation Radar (PR) providing the most accurate overland rainfall retrievals currently available from space (Kummerow et al 2000). Unlike ground-based radar and rain gauge networks, which offer unique advancements for precipitation measurement, the satellite based precipitation estimates are available over mountainous terrain, the tropical rainforests and areas covered by water.

Consequently, they represent the best available substitute for *in situ* measurements of precipitation over those regions. Nevertheless, observations from earth-orbiting satellites offer intermittent coverage over a given region of interest (currently this is approximately six to eight observations per day accounting for all available satellite platforms). There has been an effort to abridge those gaps estimating precipitation from proxy parameters, such as cloud-top temperature, that can be inferred from half-hourly geo-stationary observations of visible (VIS) and infrared (IR) radiances (Adler et al. 1988, Anagnostou et al. 1999, Levizzani et al. 2001).

Improvement of IR satellite precipitation retrievals through regional calibration by the use of microwave observations is currently approached in a number of recent studies including Hsu et al. (2000), Todd et al. (2001) and Huffman et al. (2003). This relation lies on the fact that microwave signatures are sensitive to the presence of ice and/or graupel as opposed to the IR sensor, which is mainly sensitive to cloud top characteristics (Ferraro and Marks, 1995). Nevertheless, a common observation from these studies is that satellite based rain retrievals are still limited in terms of their ability to sufficiently characterize the surface rainfall variability. This is due to the weak physical relationship of infrared measurement to convective rain processes. For example microwave-calibrated infrared techniques have been shown to be associated with significant error at high resolution (Todd et al. showed about 0.3 correlation and 350% standard error at 0.1 degree resolution in comparison with hourly radar data). At coarser resolution the retrieval error decreases significantly, for example Todd et al. showed the standard error decreasing to about 90% at 1-degree daily comparisons with radar rainfall.

To improve upon this limitation recent studies have combined satellite infrared data with lightning observations that provide surrogate information on intense thunderstorms (Goodman et al. 1988, Grecu et al. 2000, Morales and Anagnostou 2003). These studies have shown that

lightning measurements can provide reliable delineation of the convective cores in a storm, which can lead to significant improvement in determining the rainfall variability. Morales and Anagnostou (2003) in particular who developed a comprehensive scheme for continuous thunderstorm monitoring over very large regions with the use of a long-range lightning network demonstrated that in estimation of convective rain area there can be an overall bias reduction of 31% by using lightning information, while in regards to correlation, the increase in hourly estimates is about 20% for high resolution (0.1 degree and hourly) estimates. Concentrating in regions associated with higher thunderstorm frequency and improved lighting location retrieval accuracy for the receivers network, the authors were able to demonstrate that the expected improvements from lightning were even greater.

Byers (1965) has been among the first to investigate the lightning electric field produced during thunderstorms. Other pioneering studies were oriented towards the connection of lightning to precipitation from thunderstorms (Livingston and Krider, 1978; Goodman 1990; Cheze and Sauvageot, 1997; Buechler et al., 1994; Tappia et al 1998). Lightning has been correlated to cloud microphysical structure, since its presence is associated with the presence of ice polarized crystals and strong updrafts (Reap and Mac Gorman, 1988; Solomon and Baker, 1998) and/or the presence of graupel (Ahijevych, 1999). Lightning information (intensity and location) has also been used for the distinction of precipitation into convective and stratiform regimes (Houze, 1993; Zipser, 1994). A generality to be drawn from all these studies is that lightning and convective rainfall are more strongly correlated the more continental is the convection.

This paper describes a high-resolution (0.1 degree at half-hourly time scale) rainfall algorithm (henceforth referred to as Omvrios) that combines ½-hourly satellite infrared

measurements with Cloud-to-Ground (CG) lightning location and timing information from a long-range lightning network (Zeus) in Europe. The algorithm uses the lightning information to differentiate precipitation cloud systems (defined by the 255 degree K isotherm in the IR temperature array) into electrified (thunderstorms) and non-electrified (rain showers), and in determining the convective rain area and area-averaged rain rates of thunderstorm systems. The algorithm relationships are determined based on coincident rain fields derived from SSM/I passive microwave observations using a PR-calibrated and rain gauge-adjusted overland retrieval scheme (Grecu and Anagnostou, 2001). Validation is performed based on 6-hourly rainfall measurements from the European Center for Mesoscale Weather Forecasting (ECMWF) rain gauge network. The significance of the developed combined IR/lightning scheme is assessed through comparison with existing IR techniques (MW-calibrated) using the independent ECMWF rain gauge network data. Discussion of future research is offered in the conclusions section.

In the next section we discuss the data and study area. Section 3 presents the algorithm, while section 4 and 5 presents the validation and algorithm inter-comparison statistics. We close with conclusions in section 6.

2. Data

The study region covers a part of the European continent with [20N-55N] latitude and [10W-30E] longitude extend. The study period (calibration and validation) is from May to August 2002, which is a typical period for deep convective activity over Europe (Prodi et al., 2000). The satellite data used are infrared (IR) brightness temperatures from METEOSAT, and

multi-frequency (85, 37, 22, and 19 GHz) passive microwave brightness temperatures from SSM/I. The ground-based data include lightning location and timing retrievals from a long-range lightning network (Zeus) and 6-hourly rainfall reports from the ECMWF rain gauge network in Europe. The sample statistics of our compiled dataset is shown in Table 1, which includes the number of matched SSM/I-IR orbits associated with rain, the number of thunderstorm and rain shower cloud systems, the number of rainy ECMWF gauge reports and the mean rainfall and standard deviation of these 6-hourly rain gauge rainfall accumulations. In Figure 1 we show the locations of both the ECMWF rain gauges and Zeus network receivers.

The Zeus network (described in http://sifnos.engr.uconn.edu) consists of six Very Low Frequency receivers, located in Birmingham [UK], Roskilde [Denmark], Iasi [Romania], Larnaka [Cyprus], Mt. Etna [Italy], and Evora [Portugal], each sampling the time series of the vertical electric field emitted by a CG. The system retrieves the location of CG lightning activity occurring over a very large region (Europe, North Africa and part of the Atlantic and West Asia) based on the arrival time difference (ATD) method (Lee, 1986). An error analysis of Zeus lighting location retrieval based on simulation and through validation data from Spain's regional lighting network has shown that the lightning location error in Europe varies from 5 to 40 km with a mode at 20 km (Chronis and Anagnostou, 2003). From past studies (Morales, 2002) we expect the detection efficiency of this system to be high (70-90%) within the periphery of network receivers.

Estimated rainfall from SSM/I passive microwave (PM) observations was used in this study to calibrate the combined IR-lightning algorithm. The PM rain estimation was based on an overland PM retrieval scheme similar to Grecu and Anagnostou (2001). This algorithm was originally designed to estimate rain from the TMI channels based on parameters calibrated to the

most definitive PR rainfall rate and type (convective vs. stratiform) estimates used as reference. The algorithm consists of three processing stages: (1) rain area delineation, (2) convective-stratiform rain classification, and (3) estimation of rain rates for the convective and stratiform rain pixels. Rain area delineation and convective/stratiform rain classification are accomplished through a neural network scheme, which uses various features extracted from the PM brightness temperature data, while rain rate estimation is based on a multi-linear regression model applied to multi-frequency PM brightness temperatures.

There are two issues when applying the above algorithm to SSM/I data over Europe. Firstly the PR and SSM/I sensors are onboard different satellites thus, it is difficult to get an adequate collocated dataset. Secondly, TRMM satellite does not cover Europe; consequently, any developed technique would have to be transferred from a different continental region that is under TRMM coverage. To avoid the collocation problem, we remapped TMI frequencies to the SSM/I frequencies resolutions and used those as "pseudo SSM/I" data in calibrating the algorithm parameters. Re-mapping provides more data samples than directly matching PR and SSM/I orbits. The remapped TMI brightness temperatures were compared to the actual SSM/I temperatures for consistency. Figure 2 shows an example of re-mapped TMI and actual SSM/I 85-GHz channel data, which indicates that temperatures are nearly equal (within 1 degree K). Consequently, we used coincident re-mapped TMI and PR data over the continental US in the period June to September 2000 to calibrate the SSM/I overland rain retrieval. The total data used were 400,000 coincident pixels of 0.2-degree resolution, of which approximately 40,000 were rainy. The data were divided to a calibration dataset consisting of 40% of the data sample size, while the remaining 60% was used to evaluate the calibrated algorithm difference statistics with respect to PR rainfall estimates. The evaluation statistics were 0.74 in correlation, a

multiplicative bias of 1.06, and an overall 68% relative variance of the algorithm-PR rain retrieval differences.

The retrieval was applied to SSM/I data (F13/F14/F15 platforms) over Europe to estimate instantaneous convective and stratiform rainfall rates at a 0.2-degree resolution. For *in situ* validation, instantaneous SSM/I estimates were compared against coincident ½-hourly rainfall rates from a rain gauge network (72 gauges) over the Swiss Alps covering the area 6.25^{o}E to 11.25^{o}E and 45^{o}N to 48^{o}N. This validation exercise utilized data from three summer months (June-August) of 2000. There are 30,260 coincident rain gauge-SSM/I data points from this period where 4,000 of those were rainy. The unconditional (conditional, gauge>0) mean rain gauge rainfall of the coincident dataset is 0.17 (1.3) mm/hr, with a standard deviation of 0.91 (2.2) mm/hr. The SSM/I retrieval was found to correlate well with the ½-hourly gauges with a correlation coefficient of 0.74, but being biased by a factor of two as shown in Figure 3. Consequently, the retrieval was adjusted for the above bias factor making the agreement with gauges very good as shown in Figure 3 (right panel). The PR-calibrated and gauge-adjusted PM rain retrievals from SSM/I are then used to train the combined IR-lighting algorithm as discussed below.

3. Algorithm Formulation

The algorithm is designed to produce surface rainfall fields from ½-hourly IR data and CG flash density occurring within ±15 minutes of the IR time period. The algorithm is applied over the area extending from 20°N to 55°N and 10^{o}W to 30^{o}E covering part of the European continent. The algorithm produces instantaneous rain retrieval fields at 0.1-degree spatial grid

resolution, and then aggregated to coarser space-time scales (6-hourly/daily accumulations at 0.25 to 5-degree resolution). The coarser resolutions are used for algorithm validation and comparison with other satellite rain estimation techniques as described in a following section. The algorithm is classified into two processing stages described below.

a. Rain area assignment

As in Morales and Anagnostou (2003), cloud systems (defined by a threshold IR brightness temperature of 255 K) are identified in the ½-hourly IR brightness temperature array (T_{br}). Cloud clusters identified as thunderstorms (they are associated with lightning) are classified as rainy. This is because in nearly all (~99%) cloud systems existing in our database (375 out of 378) associated with lightning we could find a rainy pixel retrieved from the coincident SSM/I passive microwave data. For the non-electrified clouds (rain showers) binary decision takes place as to whether the cloud systems are rainy or not. This is function of the most frequent temperature of the cloud system ($T_{\mathrm{mod}}{}^{i}$), the variability of IR temperatures within the cloud system characterized by their standard deviation ($STD\{T_{br}^{i}\}$) and a parameter named as *Cloud Depth* ($CD_{T_{br}}^{i}$), formulated as follows:

$$CD_{T_{br}}^{i} = \frac{1}{T_{\mathrm{mod}}^{i}} \sum_{A^i} \left(T_{\mathrm{mod}}^{i} - T_{br}^{i}(u) \,|\, T_{br}^{i}(u) \le T_{\mathrm{mod}}^{i} \right) \qquad (1)$$

where A^i is the IR temperature array of cloud cluster i and u symbolizes the latitude and longitude location of the IR temperature values in that array. This parameterization is based on the fact that the convective part of a cloud system is associated with deep "cold" cores that

overshoot the surrounding anvil clouds, which are defined by the clouds modal temperature (Anagnostou et al. 1999). Hence, *Cloud Depth* is a parameter evaluating the overall depth of the convective cloud from its background temperature. A classification parameter (*RNR*) that showed ability of discriminating rainy from non-rainy rain shower cloud systems is:

$$RNR^i = STD\left\{T_{br}^i\right\} \times CD_{T_{br}}^i \tag{2}$$

Figure 5 shows the correct and false rain classification probabilities for varying *RNR* values. These probabilities are determined based on 702 (409) rainy (non-rainy) cloud clusters where we have coincident SSM/I passive microwave rain retrieval data. As shown in Figure 4, a threshold *RNR* value that balances success and false classification is 50 K, and the rain/no-rain cloud cluster classification (*CC*) is formulated as,

$$CC^i = \begin{cases} rainy & RNR^i \geq 50 \\ non-rainy & RNR^i < 50 \end{cases} \tag{3}$$

The next step is to determine the rain area for the clusters classified as rainy. The total and convective rain areas are calculated as a function of cloud type (thunderstorms vs. rain showers), the number of flashes ($CG_{flashes}$) in thunderstorm cloud systems (number of flashes within the predefined cloud-cluster), and the cloud cluster area. The total rain area (*TRA*) assignment in a thunderstorm cloud system is based on the following equation:

$$TRA^{thunderstorm} = \alpha \times A^i{}_{Cluster-Area} \tag{4}$$

where the cloud cluster area $A^{i}_{Cluster-Area}$ is defined as the cloud area delineated by the 255 K isotherm. The convective rain area (*CRA*) of the thunderstorm cloud is calculated as

$$CRA^{thunderstorm} = \beta \times \sqrt{A^{i}_{Cluster-Area} \times CG_{flashes}} \quad (5)$$

The stratiform rain area is then calculated by subtracting the convective from total rain area. In rain shower cloud systems we only determine *TRA* as in (4):

$$TRA^{rain-shower} = \gamma \times A^{i}_{Cluster-Area} \quad (6)$$

The parameter values and associated linear correlation coefficients of relations (4) through (6) are summarized in Table 2. In Table 2 we also present the parameter values and correlations for the same algorithm, but without using lightning data. A key observation from this table is that the classification based on lightning information improves the relationship between the bulk cloud system parameters and precipitation parameters. This is consistent with Morales and Anagnostou (2003) study, which involved a similar thunderstorm versus rain shower classification in their rain area delineation showing improvements in the correlation of derived parameterizations.

A schematic demonstration of the convective-stratiform area delineation procedure is provided in Figure 5. In the left panels we show a typical example of IR cloudiness (from Meteosat-7) and the recorded CG lightning by Zeus associated with a thunderstorm above the Iberian Peninsula. In the right panel we show the 255-K cloud cluster (lighter gray

discoloration), the retrieved stratiform region (medium discoloration) and the convective areas (darker discoloration) embedded within the overall rain area. Note that the retrieved convective areas are concentrated in and around the areas of high electric activity.

b. Rain rate assignment

Area-averaged rain rate values for the convective and stratiform portions of a cloud system are determined in this algorithm. The stratiform (*SRR*) and convective (*CRR*) area-averaged rain rates are calculated as function of cloud type, electrical activity (the number of flashes in a thunderstorm), the cloud depth parameter ($CD^{i}_{T_{br}}$) and the most frequent temperature (T^{i}_{mod}) of the cloud system. Hence in the case of a thunderstorm cloud type, the convective area-averaged rainfall rate is calculated as:

$$CRR^{thunderstorm} = \lambda \times T^{i}{}_{\mathrm{mod}} \times CG_{flashes} \tag{7}$$

and the stratiform area-averaged rainfall rate as

$$SRR^{thunderstorm} = \kappa \times CD^{i}_{T_{br}} \tag{8}$$

In a rainshower cloud type, the area-averaged rainfall rate of the total rain area is determined as:

$$SRR^{rain-shower} = \mu \times CD^{i}_{T_{br}} \; . \tag{9}$$

It is noted that in the rain shower cloud type, the lack of convective rain area and rate retrieval should not be interpreted as that those systems are not associated with convective rainfall, but that the retrieval based solely on IR data cannot properly used to identify convective rain rates. The parameter values of equations (7) through (9) are summarized in Table 2. It is noted that only cloud clusters colder than 255 K are considered in this study, which indicates that "warm rain" systems would be missed—this is a limitation of the retrieval.

3. Comparison with rain gauges

The algorithm rain retrieval is assessed via comparison with independent rainfall measurements from ECMWF rain gauge network. The network consists of approximately 700 tipping bucket rain gauges spread across the European continent. The data are 6-hourly cumulative rainfall records report at 06, 12, 18, and 24 (00) UTC of the day. In this study we used 49 storm days throughout the period May through August 2002. The evaluation of the algorithm is based on a number of descriptive statistics relating the algorithm retrieval (R_{est}) to rain gauge (R_{gauge}) rainfall accumulations for different space (0.1, 0.25, 0.5, 1 and 5 degree grid resolution) and time (6-hourly and daily accumulations) scales.

To statistically characterize the agreement between algorithm estimates and rain gauge measurements (considered as the ground truth) in discriminating rain from no rain, we used three performance scores: probability of detection (*POD*), false alarm rate (*FAR*) and the critical success index (CSI) determined based on 6-hourly and 0.1 degree rainfall data. The *POD* and *FAR* statistics are formulated for varying (from 0 to 30 mm) 6-hourly rain gauge ($R_{gauge}^{threshold}$) and algorithm estimated ($R_{est}^{Threshold}$) rainfall accumulation thresholds, accordingly, as:

$$POD = P\left\{R_{est} > 0 \mid R_{gauge} > R_{gauge}^{threshold}\right\} \tag{14}$$

$$FAR = P\left\{R_{est} > R_{est}^{threshold} \mid R_{gauge} = 0\right\} \tag{15}$$

Figures 6 and 7 show the *POD* and *FAR* statistics of the retrieval, presented separately for the four 6-hourly intervals of the day. There are no notable differences in the algorithm's *POD* and *FAR* scores with respect to the time of the day. The algorithm detects about 50% of the total rainfall, and over 80% (95%) of 6-hourly rainfall accumulations exceeding 20 mm (25 mm). Its overall false rain detection rate is 10%, which drops to zero for rainfall accumulation exceeding 8 mm in 6-hourly intervals. The CSI statistic is evaluated for a varying (from 0 to 30 mm) six-hourly rainfall accumulation threshold (R_{thr}) common to the gauge (R_{gauge}) and algorithm (R_{est}) rainfall estimates defined as:

$$CSI = \frac{N_1}{N_1 + N_2 + N_3} \tag{16}$$

The numerator and denominator variables are defined as:

$$\begin{aligned} N_1 &= \left\{R_{est} > R_{thr} \mid R_{gauge} > R_{thr}\right\} \\ N_2 &= \left\{R_{est} > R_{thr} \mid R_{gauge} \le R_{thr}\right\} \\ N_3 &= \left\{R_{est} \le R_{thr} \mid R_{gauge} > R_{thr}\right\} \end{aligned} \tag{17}$$

The *CSI* scores are shown in Figure 8 for the four 6-hourly time intervals of the day. We note that this parameter shows no diurnal dependence as well. The algorithm starts from a CSI score of about 0.5 at low rain accumulations, which decreases to a low value of about 0.2 at 6-hourly rain accumulations greater than 25 mm. This is a typical behavior of IR techniques, due to the weak connection of IR cloud top measurements to high rainfall rates below. As we will show in the subsequent section adding lightning information helps improve the retrieval's score.

The second group of descriptive statistics for the algorithm retrieval is the relative mean error (*MRE*) and relative root-mean-square difference (*RRMS*), the retrieval-gauge correlation (*CC*), and the overall mean retrieval error with respect to the gauge (*Bias*). The *MRE* and *RRMS* are defined as:

$$MRE = \frac{\sum_{V} \{R_{gauge} - R_{est}\}}{\sum_{V} R_{gauge}} \tag{18}$$

$$RRMS = \frac{\sqrt{\frac{1}{N_V} \sum_{V} \{R_{gauge} - R_{est}\}^2}}{\frac{1}{N_V} \sum_{V} R_{gauge}} \tag{19}$$

where V is the array of retrieval-gauge rainfall pairs defined as:

$$V = \Omega\{R_{gauge}(u), R_{est}(u) \mid R_{gauge}(u) > 0\} \tag{20}$$

where u is a common gauge-retrieval grid location for a specified space and time resolution, while N_V is the sample size of the conditional array of common (R_{est}, R_{gauge}) pairs. The correlation is evaluated based on the gauge-retrieval pair values defined in (20). The *Bias* statistic is defined as the ratio of the total (i.e., unconditional sum) gauge to retrieved rainfall. Table 3 provides an overview of the evaluated statistics for varying spatial resolution (0.1, 0.25, 0.5, 1 and 5 degrees). As shown in Table 3, decreasing the grid resolution makes the algorithm's random error (presented in *RRMS* statistic) decrease from 0.93 to 0.78. We note an unexpected moderate decrease of the retrieval random error with increasing grid size. This is due to the corresponding increase in the rain gauge area-average rainfall estimation error caused by area-point sampling uncertainty (Morrissey 1995). Table 4 shows statistics of the ECMWF gauge density for different grid resolutions. As noted in the table, increasing the grid size is associated with a moderate increase in gauge density. For example going from ½-degree to 5-degree (an order of magnitude increase in size) pixel resolution we get an average (maximum) gauge density increase from 2 (4) to 7 (9) gauges per grid, which corresponds to an increase of about 3 (2) times. Table 3 also shows that Omvrios retrieval tends to underestimate high-resolution rain rates, while it is almost unbiased at coarser scales. The overall bias (mean relative error) varies from 0.7 (18%) at 0.1-degree resolution down to about 0.95 (5%) at 5-degree grid resolution. A visual comparison between estimated rain rates and rain gauge 6-hourly rain accumulations is provided in Figure 9. The scatter plot represents corresponding rain gauge measurements and retrievals collected throughout the entire comparison period.

In the next section, the algorithm error statistics are compared against existing MW-calibrated IR rain estimation techniques to assess the significance of the use of lightning in the retrieval.

4. Significance of Lightning information – comparison with other techniques

The proposed algorithm is compared in this section against two existing MW-calibrated IR techniques. The first is a MW-calibrated IR retrieval, which is part of a variable rainfall product (VAR) array produced at NASA Goddard by Huffman et al. (2003, 2001), and is referred to as 3B41RT product (ftp://aeolus.nascom.nasa.gov). The second is a Neural Network-based technique (named Precipitation Estimation from Remote Sensed Information using Artificial Neural Networks (PERSIANN)) that combines passive microwave and Infrared observations (Hsu et al. 1997, 1999). The VAR retrieval incorporates the NOAA Climate Prediction Center ½-hourly Global Infrared composites (Janowiak et al. 2000) aggregated to 0.25-degree spatial grid resolution and hourly accumulations. The technique uses instantaneous precipitation fields from TMI and SSM/I (F13, F14 and F-15) passive microwave observations to dynamically calibrate the IR rain algorithm. The calibration is based on matching the probability density histograms of IR brightness temperatures and MW rain rates falling within a common dataset. The PERSIANN technique is based on a Neural Network algorithm that retrieves area averaged rainfall at 0.25 degree grid resolution and 6-hourly time scales by incorporating information from various data sources including the ½-hourly Global Infrared array, passive microwave rainfall maps from SSM/I and TMI, as well as ground based rainfall measurements from rain gauges and radars, and surface topographic information.

The above algorithms are selected for comparison with the developed retrieval due to their consistency with our technique, i.e., they are both calibrated to passive microwave rain rates, and they are optimal at similar space-time scales (0.25 degree in space and six-hourly in

time). The main difference of our algorithm with the above techniques is the incorporation of large regional lightning information. Consequently, such comparison would serve the purpose of evaluating the significance of lightning information in rainfall estimation from satellite Infrared data. For completeness our combined lightning/IR retrieval is also compared to a similar algorithm without considering the lightning information (i.e., all cloud systems in our database are treated as rain showers). The non-lightning algorithm parameters are shown in Table 2. We compared the combined lightning/IR and non-lightning Omvrios algorithm to the other two techniques (PERSIANN and VAR) using as common reference the 6-hourly rain accumulation measurements from the independent network of ECMWF gauges in Europe. A typical example of 6-hourly rainfall maps derived from the four techniques is shown in Figure 10. We note distinct differences among the retrieved rain maps, which are statistically investigated on the basis of rain gauge data as discussed below.

The gauge-retrieval difference statistics used in this evaluation are the ones defined in the previous section, i.e., MRE, RRMS, CC, and Bias, evaluated both conditionally ($R_{gage}>0$ in Eq-20) and unconditionally ($R_{gage} \geq 0$ in Eq-20) with respect to gauge rainfall. The algorithm inter-comparison statistics are summarized in Table 5. The conditional versus unconditional systematic difference of Omvrios retrieval with gauges is shown to vary by only 5%, while for the PERSIANN and VAR techniques the variation is more significant, i.e., 75% and 34%, respectively. The Omvrios algorithm is associated with lower random differences against gauges (i.e., RRMS) compared to the other techniques in both conditional and unconditional differences. In particular, the Omvrios offers a 41% (25%) reduction in conditional RRMS with respect to the PERSIANN (VAR) method, while the reduction in the unconditional RRMS is 36% (65%). The improvement due to lightning is also apparent in the comparison of the correlation statistic

between the different methods. It is shown that the conditional correlation between Omvrios retrieval and gauges is higher by about 0.3 (0.24) compared to the PERSIANN (VAR) method. Similar improvement is also shown for the unconditional correlation. We further compared the different algorithms presenting the Critical Success Index evaluated against gauge rainfall for different rainfall thresholds. The comparison is presented in Figure 11 where we show that Omvrios algorithm is associated with higher CSI values for almost the whole range of 6-hourly rainfall accumulation threshold values. The higher CSI statistic indicates that the algorithm is more efficient (higher POD and lower FAR) in detecting rainfall accumulation exceeding the threshold values at 0.25-degree and 6-hourly space-time scales. Finally, in Figure 12 we show cumulative probability histograms of all four retrievals and rain gauge accumulations. It is apparent that the combined IR/lightning retrieval cumulative rainfall histogram resembles closer the rain gauge rainfall histogram, which strengthen our hypothesis that lightning helps improve IR rainfall estimation. It is noted that the quantitative interpretation of the inter-comparison results is tight to the scales presented in this study, and can only qualitatively be generalized at other scales (especially at higher spatial-temporal resolutions).

5. Conclusions

This study has presented a passive microwave-calibrated combined IR/lightning (Omvrios) retrieval applied over Europe. IR cloud systems delineated by the 255 K isotherm in the IR temperature array were classified in two types: thunderstorms (electrified) and rain showers (non-electrified). The retrieval is based on bulk parameterizations that relate cloud top IR temperature and lightning characteristics to rain/no-rain discrimination of the cloud system,

rain area (total and convective rain area) delineation and finally the associated convective and stratiform area-averaged rain rates. The technique was calibrated based on coincident rain fields derived from a PR-calibrated and gauge-adjusted SSM/I rain estimation algorithm. The retrieved rain rates were aggregated to 0.1-degree grid resolution and 6-hourly temporal accumulation. The algorithm has been validated and compared to existing microwave-calibrated IR retrievals using independent six-hourly rain accumulation measurements from a rain gauge network spread across Europe.

The main conclusions from the algorithm validation are as following. Its systematic difference with gauges decreased from 30% at 0.1-degree resolution to a 5% at 5-degree resolution. The relative root mean square difference decreased from 93% (0.1 degree) to 78% (5 degrees), while the corresponding correlation increased from 0.78 to 0.95. There is no diurnal effect apparent in the algorithm's rain detection and false alarm probabilities. The retrieval would detect about 50% of the total rainfall, and over 80% (95%) of rainfall accumulations exceeding 20 mm (25 mm) in a six hourly interval. Its overall false rain detection rate was 10%, which drops to zero for rain accumulations exceeding 8 mm in a 6-hourly interval.

The main conclusion from the algorithm inter-comparison study is that lightning information helps reduce IR retrieval uncertainty. It was shown that the combined lightning/IR retrieval (Omvrios) had the highest critical success index score compared to the other techniques. In retrieval-gauge statistics it was shown to have significantly lower (25%-40%) root mean square differences compared to the other IR retrievals, and a nearly 0.3 increase in correlation with gauges. In terms of systematic differences, the combined lightning/IR retrieval's conditional and unconditional mean relative error values were nearly equal (within 5%), while for the other

IR rain retrievals the unconditional and conditional mean relative errors differed significantly (34% to 75%).

The exclusive use of PM or IR would not unravel the problem of rain estimation, especially over land. An alliance between these two measurements provides a head start since they are both providing information about completely different properties of the hydrometeors (dielectric properties, molecular resonance etc.) (Ulaby, 1981). On the other side lies the information on lightning. Atmospheric electricity and its formulation through a lightning stroke are important to be taken into consideration since by default, the overland rain estimation problem is ill posed. The improvements shown with the proposed method depend on the following essential reasons:

(1) Lightning can abridge the gap between IR/PM information since it's observation is continuous on one hand and directly related to precipitation microphysical properties. Moreover lightning is proven able to pinpoint convective status inside a storm cloud. Some cloud top properties seem to have a linear and direct correlation with whether a cloud is electrified or not and such distinction is proven useful in the rain/no rain decision scheme. Lightning seems also to have good and straightforward correlation with rain rate (at lower spatial/temporal resolutions) in the convective part of the cloud cluster. All cloud cluster area statistics show stronger correlation in the case of electrified clouds. The comparison of Omvrios algorithm against the same method, but in the absence of lighting information, strengthens the initial hypothesis; lightning can improve the rain detection, especially in higher rain accumulation values.

(2) Ombrios algorithm is estimating rainfall only over a limited grid covering Europe, fact that possibly smoothes out errors associated with the application of the algorithm over a

larger area (note that the other methods used for comparison, produce rain estimates for the entire Globe). Furthermore, the use of PM rain retrievals, which were adjusted to gauges in the area of Swiss Alps, may have also contributed to the better performance of Omvrios relative to the other techniques that used probably less accurate PM rainfall estimates in the calibration phase.

On the other hand, in the absence of lightning information, a more fuzzy distinction between storm clouds takes place resulting sometimes in poor rain detection especially in frontal or warm rain scenarios. So far research in electrified warm-cloud-processes is not well established. In this work, a non-electrified cloud cannot be delineated into convective/stratiform and such fact produces uncertainties that may lead to magnified errors in the estimated output. The uses of lightning as a tool for rain estimation has to always take into account the extent of spatial and time scales. That is a direct attempt to use lightning as a primary rain estimator may fail, or lead to erroneous results, since as shown spatio-temporal correlation can be high only at lower resolutions.

Future research will include extension of the herein algorithm development study over Africa using lightning data from a recently extended network of Zeus receivers in the continent. Zeus data from Africa would be widely available after the summer of 2004. Our high-frequency retrieval based on the combined IR/lightning data over Africa would facilitate a number of studies including research on African monsoon convective system dynamics and microphysics, and investigating the role of surface conditions (e.g. soil moisture and vegetation) on the regional water cycle variability. The later is currently being researched over Europe using an uncoupled land data assimilation system driven by Omvrios precipitation fields where we seek to provide improved land surface boundary conditions to a mesoscale meteorological model.

Acknowledgements: This study was supported by *NASA TRMM Project*. The first author was supported by a *NASA Earth System Science Graduate Student Fellowship*. Zeus long-range lightning network was funded by the *Greek General Secretariat for Research and Development* through a 'Center of Excellence' grant to the National Observatory of Athens (NOA). NASA Goddard-DAAC provided the Infrared data. The VAR and PERSIANN rain retrieval fields over Europe were downloaded from the author's web pages **(**ftp://aeolus.nascom.nasa.gov/pub and http://hydis.hwr.arizona.edu/precip/). Dr. Anastatios Papadopoulos of the National Marine Research Center of Greece provided the ECMWF rain gauge data.

6. References

Adler, R. F, Negri, A.J., Keehn, P. R, and Hakkarinen, I. M., 1993: Estimation of monthly rainfall over Japan and surrounding waters from a combination of low-orbit microwave and geo-synchronous IR data. J. Appl. Meteor., 32, 335-356.

Adler, R. F. and Negri, A. J., 1988: A satellite infrared technique to estimate tropical convective and stratiform rainfall, J. Appl. Meteor., 27, 30-51.

Ahijevych, A. D., 1999: Radar and Electrical Observations of MCTEX Thunderstorms, 29th Conference on Radar Meteorology.

Alexander, G. D., J. A. Weinman, J. A, Karyampudi, V. M, Olson, W. S, Lee, A. C., 1999: The effects of assimilating rain rates derived from satellite and lightning on forecasts of the 1993 superstorm. *Mon. Wea. Rev.*, 127, 1433-1457.

Arkin, P.A., 1979. The relationship between the fractional coverage of high cloud and rainfall accumulations during GATE over the B-array. *Mon. Wea. Rev.*, **107,** 1382-1387

Anagnostou, E.N, Negri A.J., Adler, R.F, 1999: A satellite infrared technique for diurnal rainfall variability studies, Journal of Geophysical Research, Vol. 104, NO.D24, pages 31, 477-31,488.

Buechler, D. E., Christian, J.H., Goodman, J.S, 1994: Rainfall Estimation using lightning data. 7th Conf. Satellite Meteor. And Ocean., Amer. Meteor. Soc., June 6-10, pp. 171-174.

Byers, H. Elements of Cloud Physics. Chicago: University of Chicago Press, 1965

Carpenter, T.M., Georgakakos, K. P and Sperfslage, J. A., 2001: "On the Parametric and Nexrad-Radar Sensitivities of a Distributed Hydrologic Model Suitable for Operational Use," Journal of Hydrology, 253, 169-193.

Cheze, J.L., and Sauvageot, H., 1997: Area average rainfall and lightning activity, J. Geophys. Res., 102, 1707-1715. clouds. *J. Atmos. Sci., 22*, 79-84.

Chronis, T. and E.N., Anagnostou, 2003: Error Analysis for a Long-Range Lightning Monitoring Network of Ground-Based Receivers in Europe. *Journal of Geophysical Research-Atmospheres (in press).*

Ferraro, R. R., and G. Marks, 1995: The development of SSM/I rainrate algorithms using ground-based radar measurements. *J. Atmos. Oceanic Technol.,* **12,** 755–770.

Georgakakos, A.P., Mullusky, M.G., Yao, H., and Georgakakos, K. P., 1998: Impacts of climate variability on the operational forecast and management of the upper Des Moines River basin. Water Resource Research, 34(4), 799-821.

Goodman, J.S., 1990: Predicting thunderstorm evolution using ground based lightning detection networks. NASA Tech Memo. TM-103521.

Goodman, S. J., Buechler, D. E. and Meyer, P. J., 1988: Convective tendency images derived from a combination of lightning and satellite data. *Wea. Forecasting*, 3, 173-188.

Grecu, M., Anagnostou, E.N., Adler, R.F., 2000: Assessment of the Use of Lightning Information in Satellite Infrared Rainfall Estimation, Journal of Hydrometeorology, pp, 211-221.

Grecu M. and Anagnostou, E.N., 2001: Overland Precipitation Estimation from TRMM Passive Microwave Observations, Journal of Applied Meteorology, 40 (8), 1367-80.

Houze, R. A., Jr., 1993: Cloud Dynamics. Academic Press, pp., 573.

Hsu, K., Gupta, H., Gao, X., Sorooshian, S., 1999: Estimation of Physical Variables from Multichannel remotely sensed imagery using a neural network: application to rainfall estimation. *Water Resources Research*, 35, 5, 1605-1618.

Hsu, K., Gao, X., Sorooshian, S. and H. V. Gupta, 1997: Precipitation Estimation from Remotely Sensed Information using Artificial Neural Networks", *Journal of Applied Meteorology*, 36(9), pp. 1176-1190.

Huffman, G. J, Adler, R.F, Morrisey, M.M, Bolvin, D.T, Curtis, S, Joyce, R., McGavock, B., Susskind, J., 2001: Global Precipitation at One Degree Daily Resolution from Multisatellite Observations, Journal of Hydrometeorology, Vol.2, pp, 36-60.

Huffman, G.J., R.F. Adler, E.F. Stocker, D.T. Bolvin, E.J. Nelkin, 2003: Analysis of TRMM 3-Hourly Multi-Satellite Precipitation Estimates Computed in Both Real and Post-Real Time. 12th Conf. on Sat. Meteor., 2 and Oceanog., 9-13 Feb. 2003, Long Beach, CA.

Janowiak, J.E., R.J. Joyce, and Y. Yarosh, 2000: A real-time global half-hourly pixel resolution infrared dataset and its applications, *Bull. Amer. Meteor. Soc*., 82, 205-217.

Kummerow, C., J. Simpson, O. Thiele, W. Barnes, A.T.C., Chang, E. Stocker, R.F.Adler, R.F., Hou, A., Kakar, R., Wentz, F., Ashcroft, P., Kozu, T., Hong, Y., Okamoto, K., Iguchi, T., Kuroiwa, H., Im, E., Haddad, Z., Huffman, G., Ferrier, B., W.S.Olson, Zipser, E., Smith, E.,A., Wilheit, T. T., North, G., Krishnamurti, T., Nakamura, K., 2000: The status of Tropical Rainfall Measuring Mission (TRMM) after two years in orbit. J. Applied Meteorology (TRMM special issue), J. Appl. Meteorol., 39, (12)Pt.1, 1965-1982.

Levizzani,V., Schmetz, J., Lutz, H. J., Kerkmann, J., Alberoni, P. P and Cervino, M., 2001: Precipitation estimations from geostationary orbit and prospects for METEOSAT Second Generation. *Meteor.Appl.*, 8, 23-41.

Livingston J. M and E.P Krider, Electric field produced by Florida thunderstorms, Journal of

Geophysical Research, vol 83, pp. 385-401, 1978

Morales, C., and Anagnostou, E.N., 2003: Extending the Capabilities of High-Frequency Rainfall Estimation from Geostationary-Based Satellite Infrared via a Network of Long-Range Lightning Observations, Journal of Hydrometeorology, 4(2), 141-159.

Morales, C., 2001: Continuous Thunderstorm Monitoring: Retrieval of Precipitation Parameters from Lightning Observations, Ph.D. Thesis, Department of Civil and Environmental Engineering, University of Connecticut, Storrs, CT 06269, pp 231.

Morrisey, M.L, J.A. Maliekal, J.S. Greene and J. Wang, 1995: The uncertainty of simple averages using rain gauge networks. Water Res. Bulletin 29, pp 855-861.

Prodi, F., Porcu, F., Natali, S., Caracciolo, C., Capacci, D, 2000: Proceedings of the 2nd EGS Plinius Conference on Mediterranean Storms, Siena, Italy.

Reap, R.M., MacGorman D.R., 1988: Cloud-to-Ground Lightning: Climatological characteristics and relationships to model fields, radar observations and severe local systems, Month. Wea. Rev., VOL 117, pp 518-535.

Simpson, S., Adler, F.R., and North, R.G., 1988: A proposed tropical rainfall measuring mission. Bull. Amer. Meteor. Soc., 69, 278-295.

Solomon, R., and Baker, M., 1998: Lightning flash rate and type in convective storms, J. Geophys. R., VOL. 103, NO.D12, PAGES 14,041-14,057.

Tapia, A., J. A. Smith, and M. Dixon, 1998: Estimation of convective rainfall form lightning observations. *J. Appl. Meteor.*, 37, 1497-1509.

Todd, M.C., Kidd, C., Kniveton, D., Bellerby, T.J., 2000: A Combined Satellite Infrared and Passive Microwave Technique for Estimation of Small Scale Rainfall, Journal of Atmospheric and Oceanic Technology, Vol. 18, pp, 742-754.

Ulaby, T. F., Moore, K. R., Fung, K.A., Microwave Remote Sensing, Volume 1, 1981

Williams, E. R., M. E. Weber, R. E. Orville, 1989: The relationship between lightning type and convective state of thunderclouds. *J. Geophys. Res., 94* (D11), 13,213-13,220.

Zipser, E.J., 1994: Deep cumulonimbus cloud systems in the Tropics with and without lightning. Mon. Wea. Rev., 122, 1837-1851.

TABLES

Table 1: Data sample statistics

# of SSM/I total orbits analyzed	345 (F-13, F-14 and F-15)
# of thunderstorm cloud clusters	434
# of rain shower cloud clusters	268
# of ECMWF (rainy) 6-hourly gauge measurements	18,812
Conditional mean gauge rainfall (mm/6h)	3.93
Conditional standard deviation (mm/6h)	9.02

Table 2: Algorithm parameter values determined in the calibration phase. The collocation grid resolution used here is 0.10 by 0.10 degrees.

Parameter	Value (Lightning is considered)	Regression Correlation	Value (Lightning is not considered)	Regression Correlation
α	0.15	0.77	0.09	0.50
β	0.027	0.6	-	-
γ	0.10	0.56	-	-
κ	1.09	(0.55)	-	-
λ	0.0005	0.70	1.25	0.43
μ	0.75	0.56	-	-

Table 3: Omvrios retrieval validation statistics against six-hourly ECMWF gauge rainfall accumulation measurements.

Grid Resolution / ***Statistic***	***0.1 deg***	***0.25 deg***	***0.5 deg***	***1 deg***	***5 deg***
MRE	0.18	0.11	0.1	0.09	0.05
RRMS	0.93	0.91	0.89	0.85	0.78
Bias	0.7	0.88	0.91	0.94	0.95
CC	0.78	0.88	0.89	0.92	0.95

Table 4: ECMWF gauge density (number of gauges per grid) per grid size.

Grid size	***0.1 deg***	***0.25 deg***	***0.5 deg***	***1.0 deg***	***5.0 deg***
mean (max) number	1 (2)	1 (2)	2 (4)	3 (6)	7 (9)

Table 5: Gauge difference statistics for the algorithm inter-comparison study. The statistics are determined at 0.25 deg grid size and 6-hourly accumulations.

Algorithm / ***Statistics (conditional/unconditional)***	***PERSIANN***	***VAR***	***Omvrios***	***Omvrios/No Lightning***
MRE	-0.87 / -0.12	-0.36 / -0.7	0.16 / 0.11	0.23 / 0.21
RRMS	1.68 / 1.42	1.31 / 2.59	0.99 / 0.91	1.05 / 1.01
Bias	1.87 / 1.13	1.36 / 1.69	0.83 / 0.88	0.75 / 0.79
CC	0.49 / 0.51	0.54 / 0.44	0.78 / 0.74	0.66 / 0.68

FIGURE CAPTIONS

Figure 1: The ECMWF rain gauge network (crosses) and Zeus lightning receivers network (solid squares).

Figure 2: Upper panels: Comparison of remapped TMI and coincident SSMI brightness temperature data. Lower panels: histograms of original SSM/I versus remapped TMI (red line) data.

Figure 3: Scatter plot of area-averaged (over the Swiss gauge coverage regime) instantaneous SSM/I rainfall retrieval versus averaged 1/2-hourly gauge rainfall. Left and right panels correspond to un-adjusted and bias adjusted SSM/I rainfall estimates, respectively.

Figure 4: Probability of successful detection of rainy and non-rainy cloud systems versus *RNR* discrimination parameter value.

Figure 5: Left panel: IR cloudiness overlaid with CG lightning locations measured by Zeus. Right panel: the delineated 255-K cloud cluster (lighter gray discoloration) overlaid by the retrieved stratiform (medium discoloration) and convective (darker discoloration) rain areas.

Figure 6: Omvrios POD scores versus rain gauge rainfall threshold presented for different time intervals of the day.

.

Figure 7: Omvrios FAR scores versus rainfall threshold presented for different time intervals of the day.

Figure 8: Omvrios CSI scores versus rainfall threshold presented for different time intervals of the day.

Figure 9: Scatter plot of Omvrios retrieval versus coincident 6-hourly rain gauge rainfall accumulations at 0.25-degree resolution.

Figure 10: Retrieved 6-hourly rainfall maps from Omvrios (upper left panel), Omvrios/No-Lightning (upper right panel), VAR (lower left panel) and PERSIANN (lower right panel) techniques.

Figure 11: CSI scores versus rain threshold presented for Omvrios, Omvrios/No-Lightning, VAR and PERSIANN techniques.

Figure 12: Cumulative rainfall histograms of Omvrios, Omvrios/No-Lightning, VAR and PERSIANN technique rainfall retrievals and six-hourly rain gauge rainfall accumulation at 0.25-degree resolution.

FIGURES

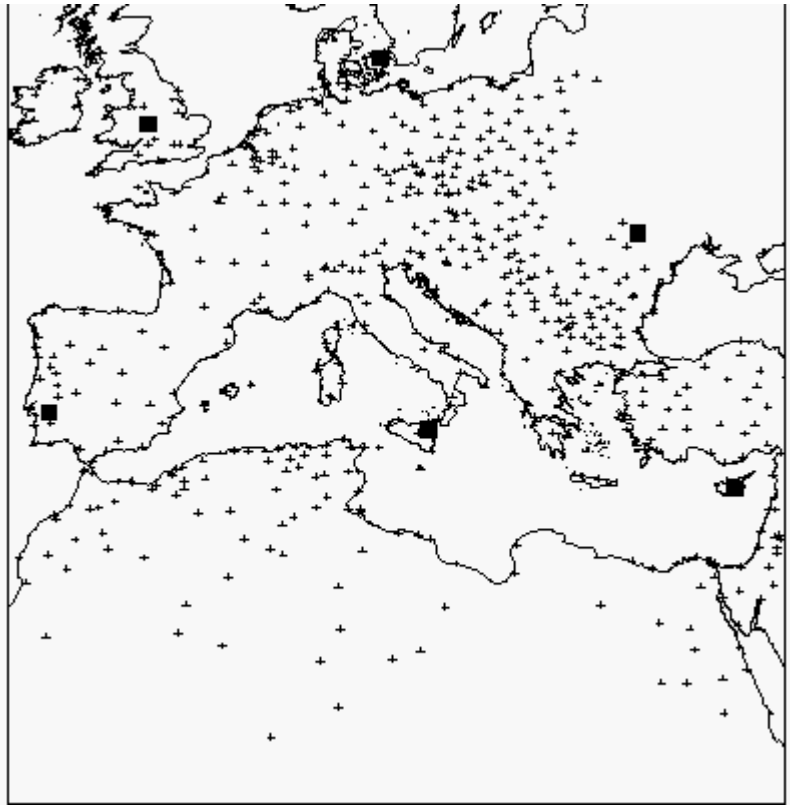

Figure 1

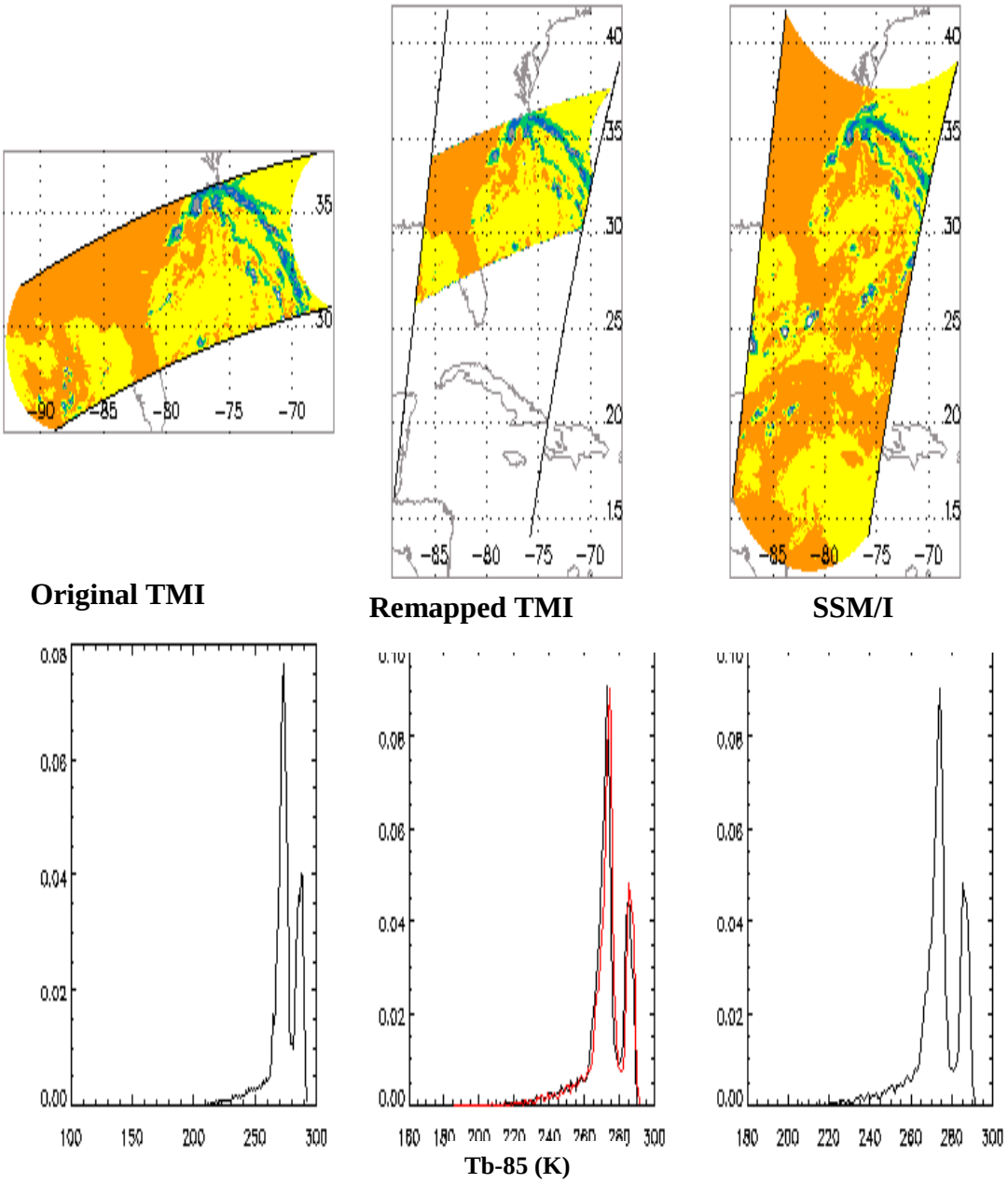

Figure 2

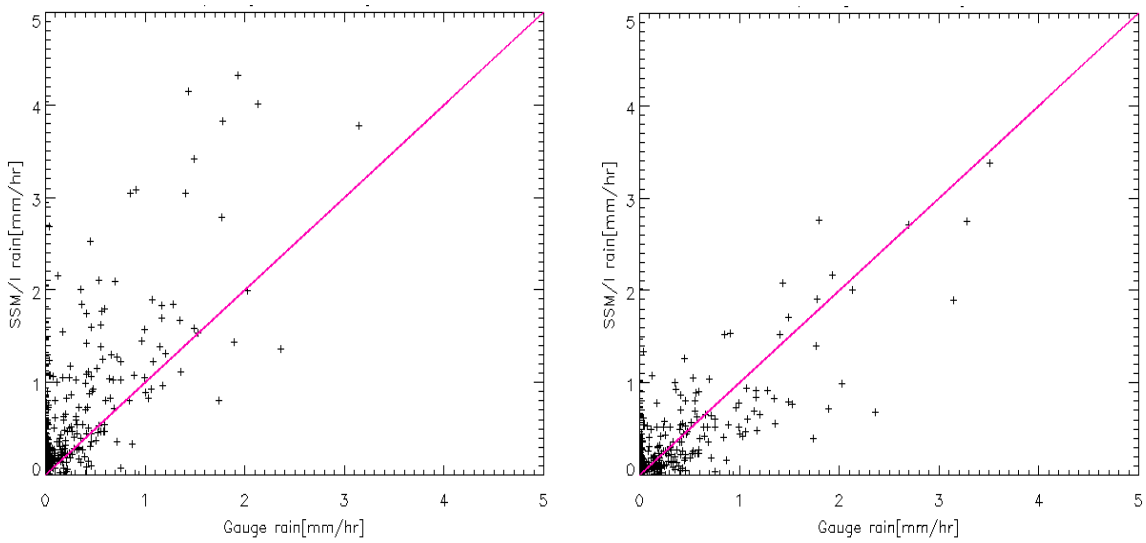
SSM/I rain[mm/hr]
Gauge rain[mm/hr]
0
1
2
3
4
5
SSM/I rain[mm/hr]
Gauge rain[mm/hr]

Figure 3

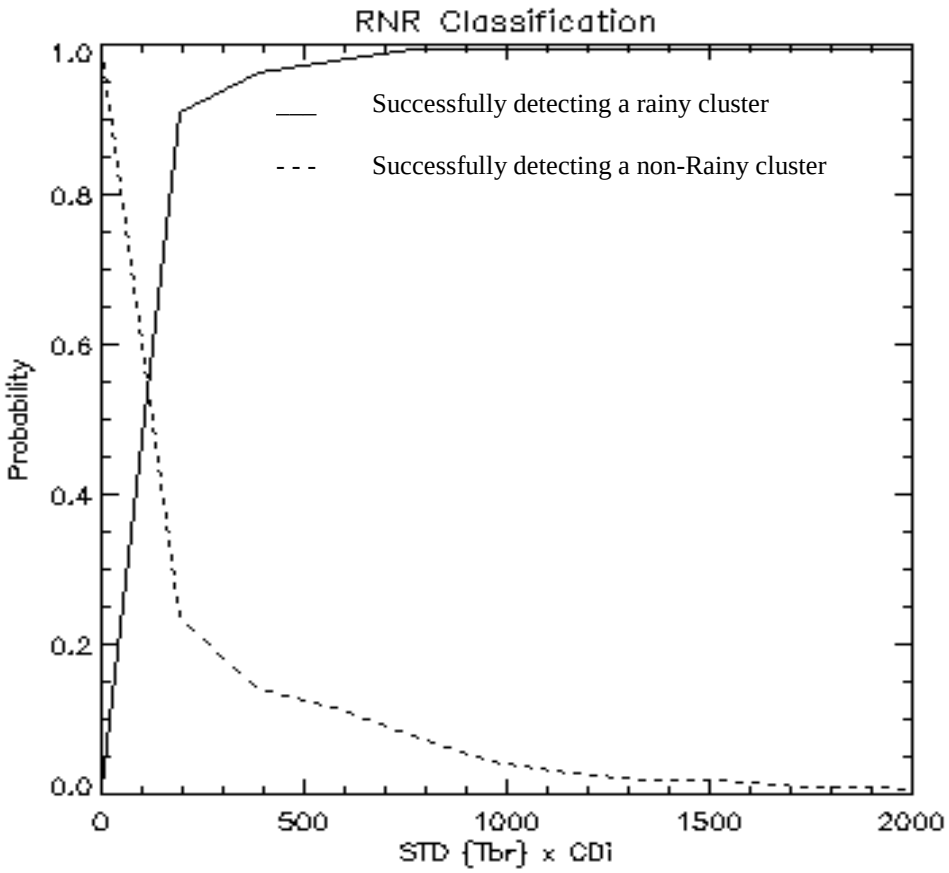
RNR Classification
Successfully detecting a rainy cluster
Successfully detecting a non-Rainy cluster
Probability
1.0
0.8
0.6
0.4
0.2
0.0
0
500
1000
1500
2000
STD {Tbr} x CDi

Figure 4

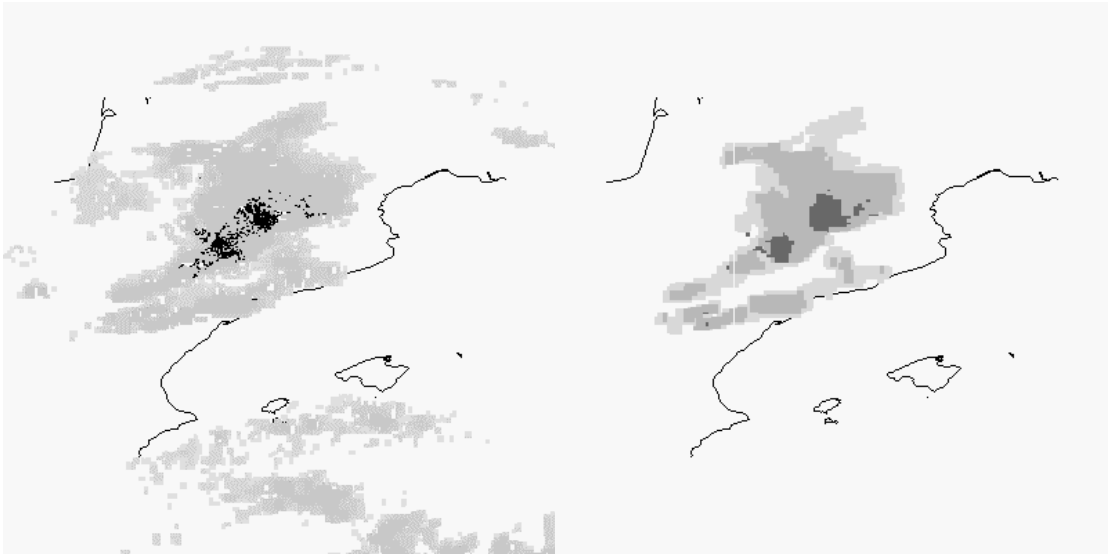

Figure 5

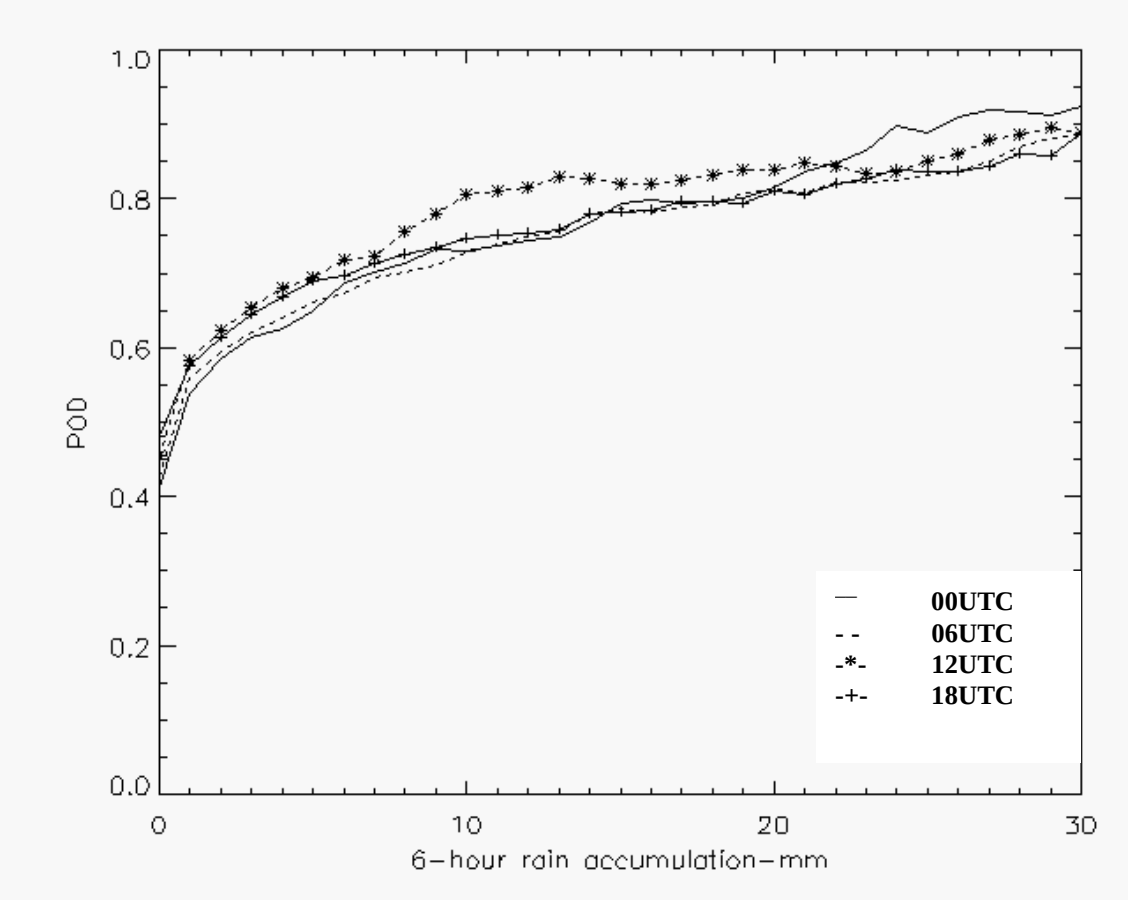
1.0
0.8
0.6
0.4
0.2
0.0
POD
0
10
20
30
6-hour rain accumulation-mm
00UTC
06UTC
12UTC
18UTC

Figure 6

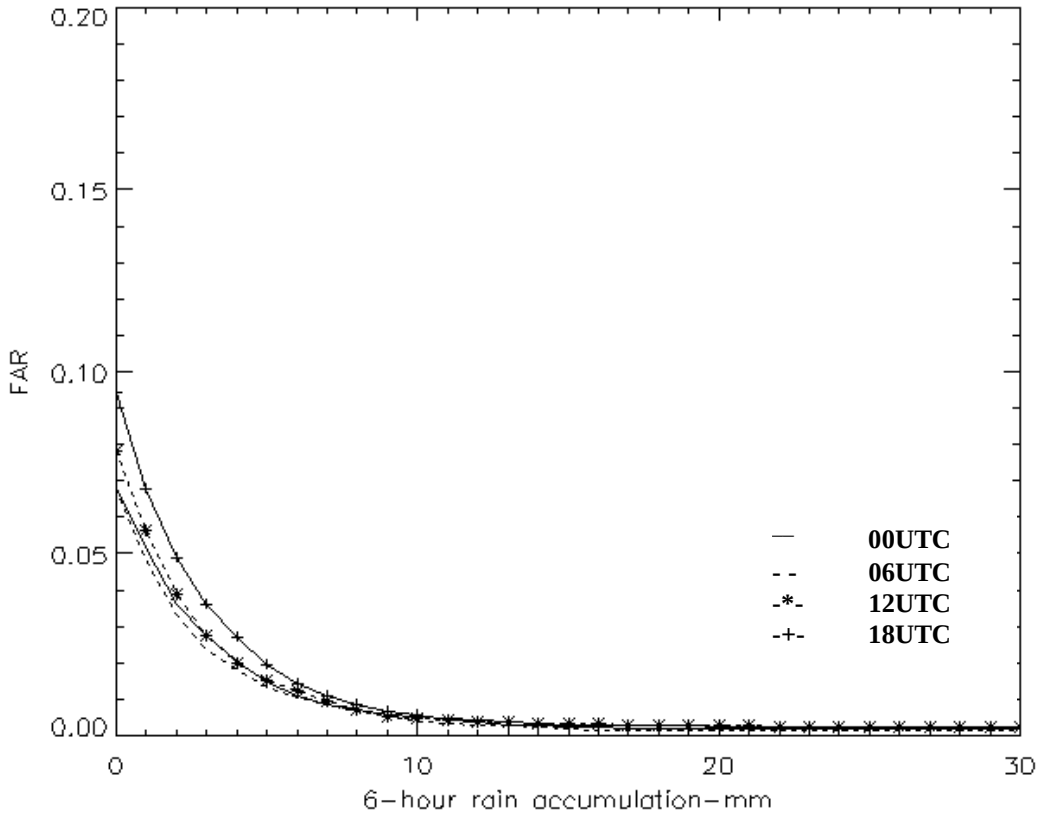
0.20
0.15
0.10
0.05
0.00
FAR
0
10
20
30
6-hour rain accumulation-mm
00UTC
06UTC
12UTC
18UTC

Figure 7

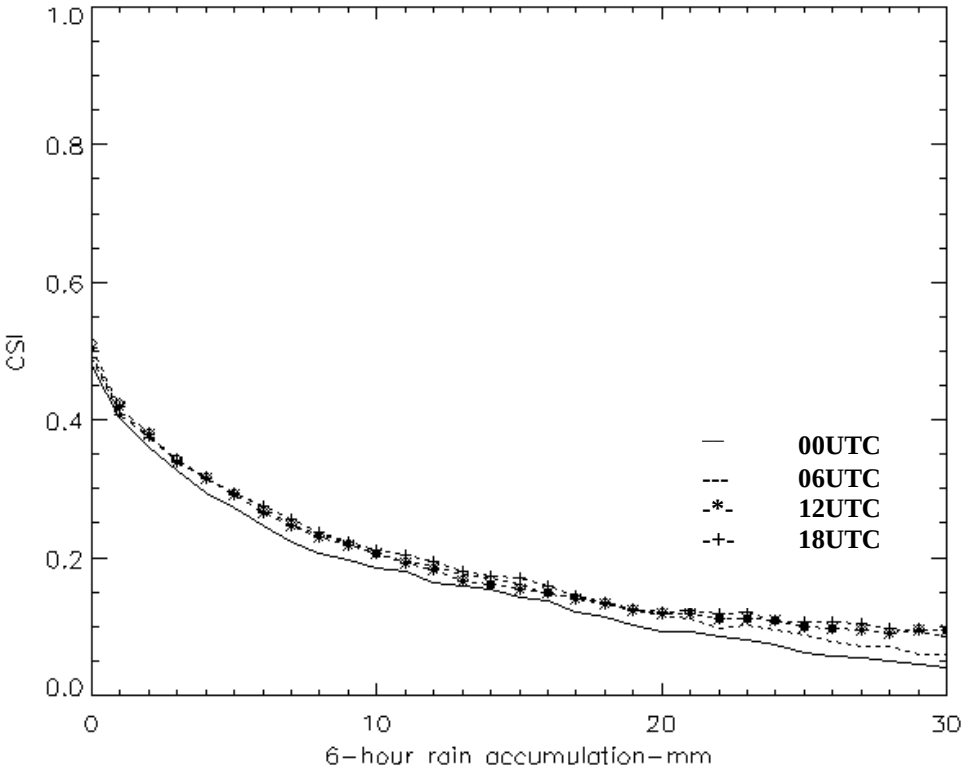
1.0
0.8
0.6
0.4
0.2
0.0
CSI
0
10
20
30
6-hour rain accumulation-mm
00UTC
06UTC
12UTC
18UTC

Figure 8

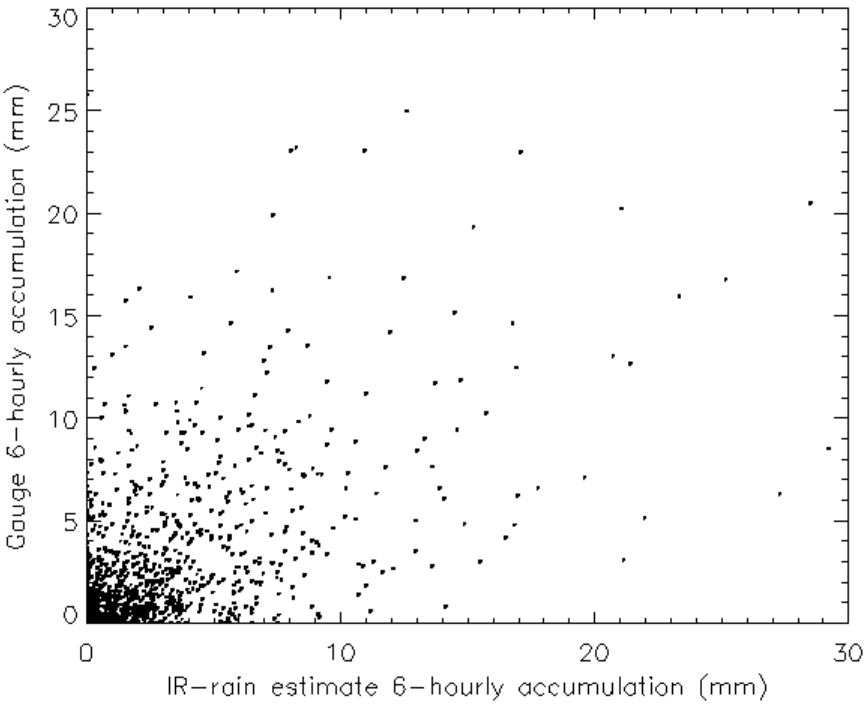
Gauge 6-hourly accumulation (mm)
IR-rain estimate 6-hourly accumulation (mm)
0
5
10
15
20
25
30
0
10
20
30

Figure 9

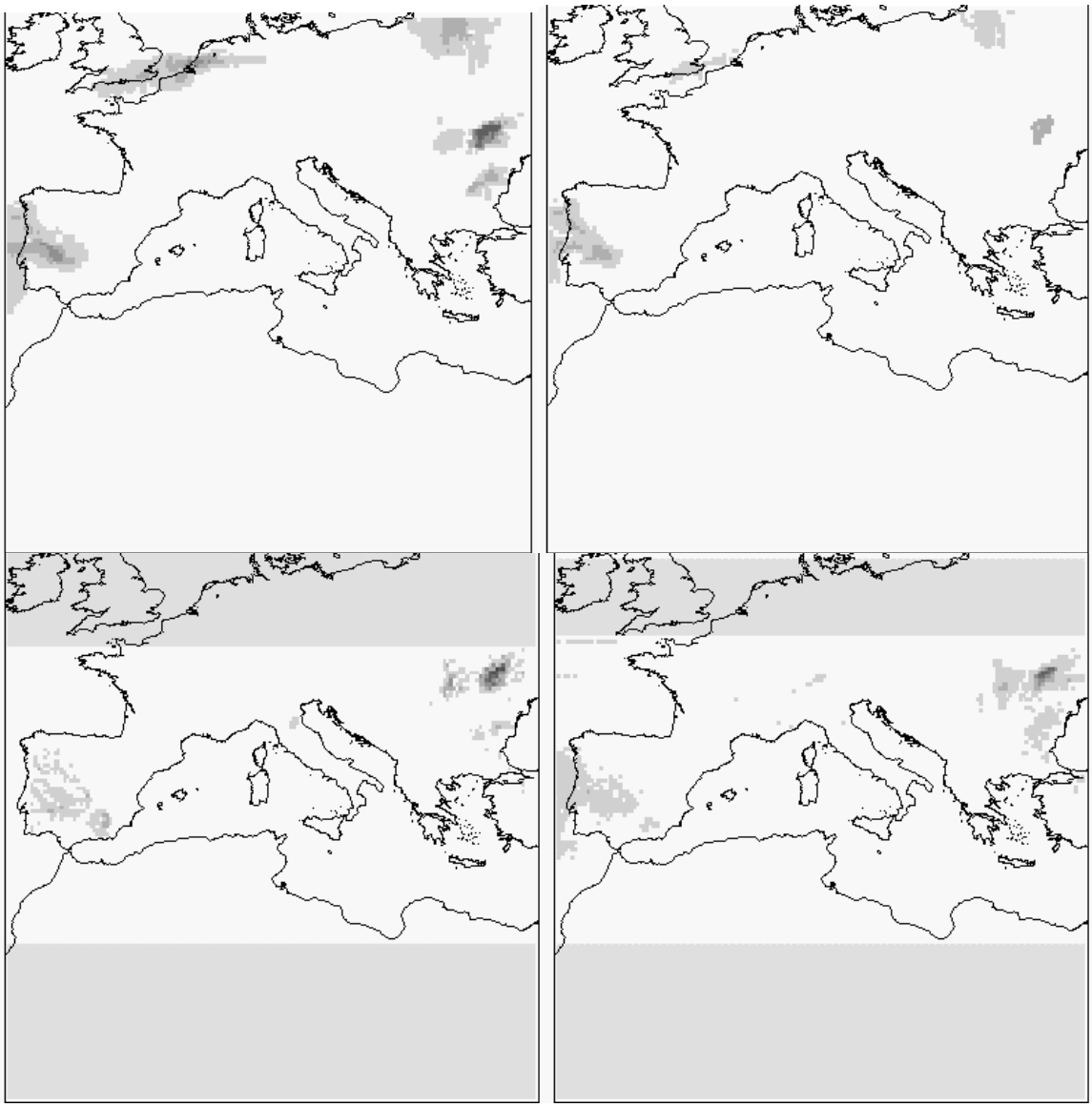

Figure 10

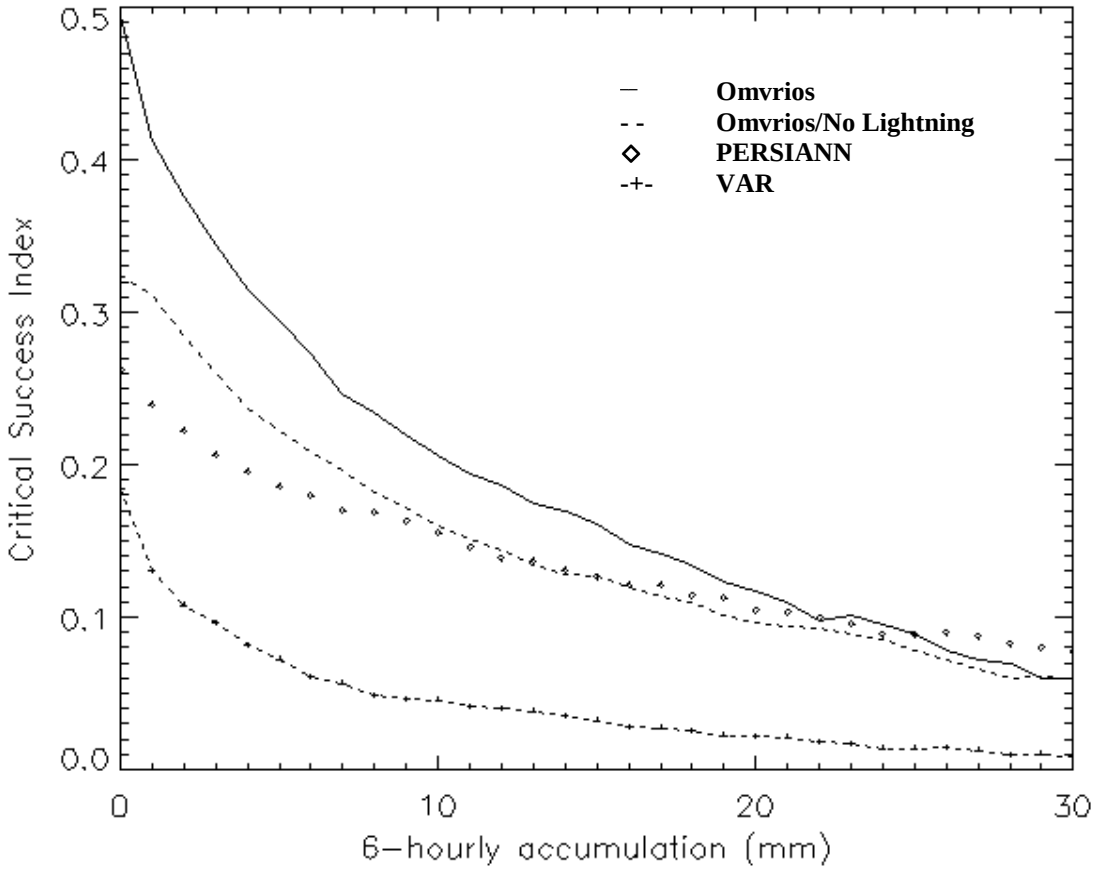
Omvrios
Omvrios/No Lightning
PERSIANN
VAR
Critical Success Index
0.0
0.1
0.2
0.3
0.4
0.5
0
10
20
30
6-hourly accumulation (mm)

Figure 11

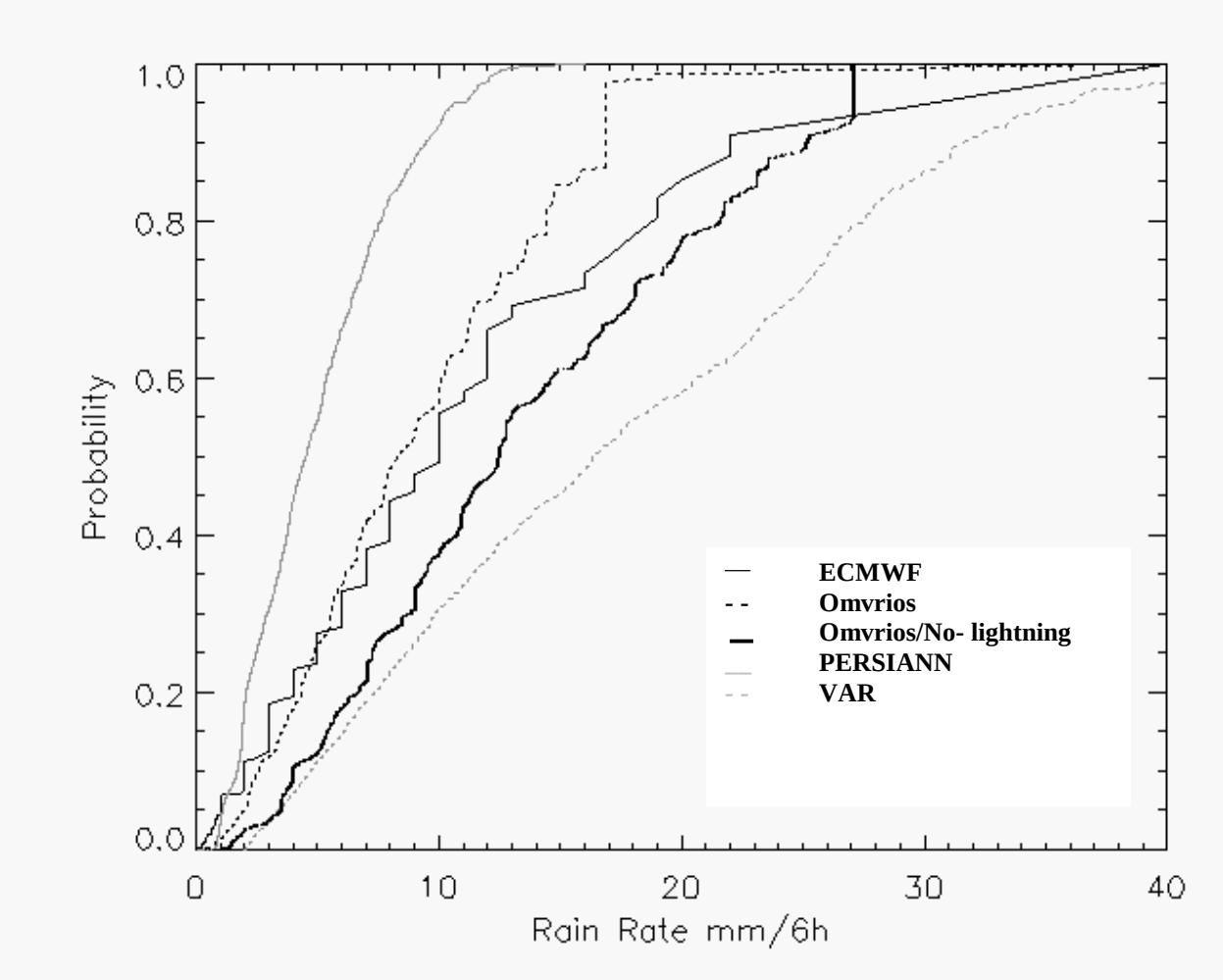
1.0
0.8
0.6
0.4
0.2
0.0
Probability
0
10
20
30
40
Rain Rate mm/6h
ECMWF
Omvrios
Omvrios/No- lightning
PERSIANN
VAR

Figure 12